An Experiment - measure and understand transport processes in a plasma.

Contents

The point of this section is to show an example of up to date, important physics which is being pursued, what must be measured, and to list some diagnostics which are used for these measurements

Three important vugraphs from a recent invited lecture.

These examples pertain specifically to a hot fusion - oriented plasma experiment. They are used only as an example. The diagnostics to be discussed are of general use, as will be pointed out as we go along.

Vu-graph 1.

A summary of edge turbulence and transport studies on different types of device.

$$\Gamma_{SOL} = \frac{n_e c_s L_n}{2 L_c}$$

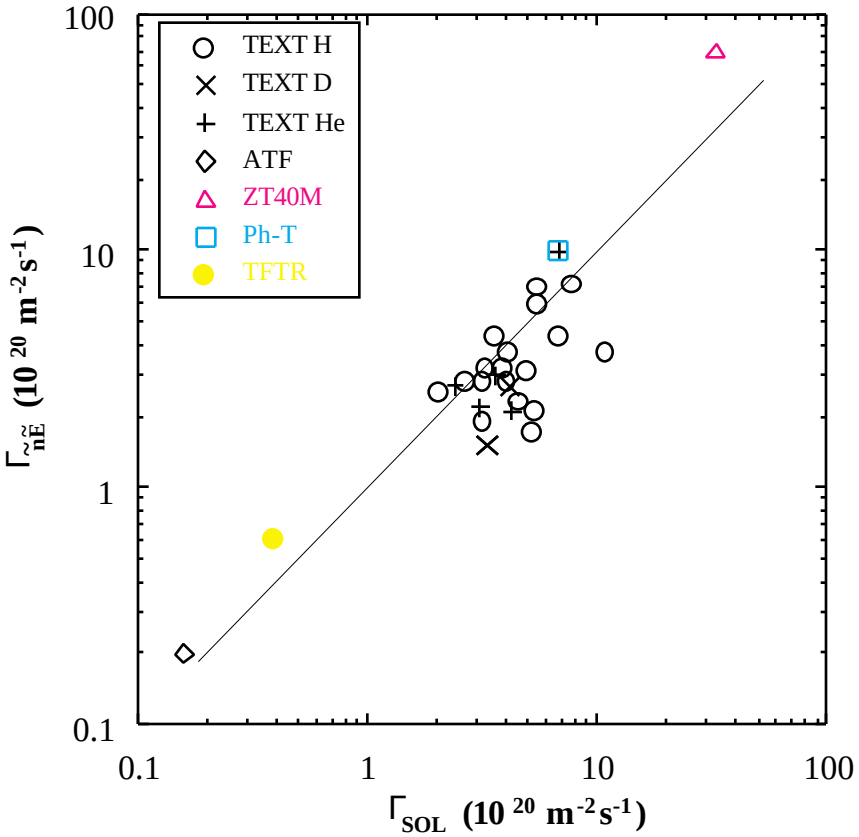

· Electrostatic turbulence "explains" total particle flux.

· This is true for tokamaks, RFP's, stellarators.

Vu-graphs 2 and 3.

Interior turbulence and transport studies (heat)

The possibilities

1. Magnetic perturbations: parallel particle motion along field lines with a component out of the flux surface.

2. Electrostatic ***ExB*** drifts across flux surfaces.

· Determine relevance of each: Compare total (heat) flux or (thermal heat) diffusivity with measured fluctuation driven (heat) flux or (thermal heat) diffusivity.

· Cannot do this, so resort to models and upper limits.

Estimated Heat Flux

- Previous estimates showed electrostatic fluctuations could not account for measured heat flux.
  - long wavelength modes only
- Recent estimates may account for heat flux
  - new measurements of $\bar{k}_\theta$
  - modeling of measured spectra to account for sample volume attenuation
  - includes poloidal asymmetry
  - assumes optimum phase between $\tilde{T}_e$ and $\tilde{n}_e$

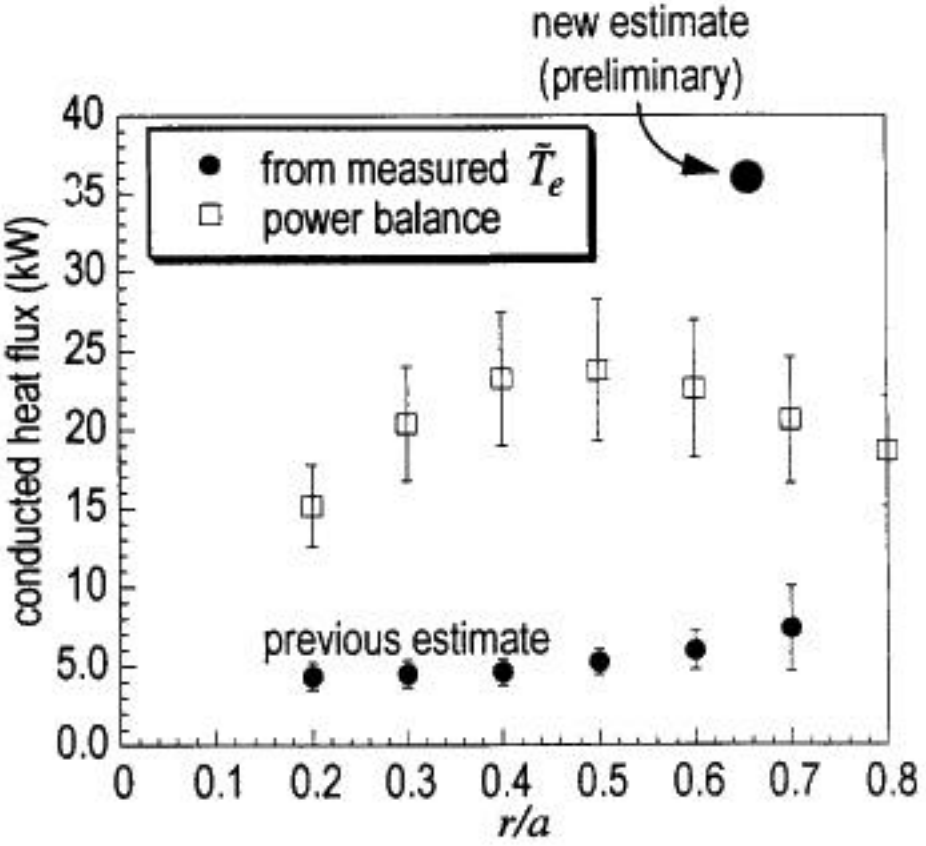

What we have just talked about

Total Fluxes

Consider the transport of particles, momentum, and energy. We are interested in the rate of change of these quantities, for example how particles cross a plasma, how energy or heat gets out from the center of the plasma to whatever is the 'wall'. Just as in any other phase, we talk about coefficients of diffusion, viscosity and conduction. We have to distinguish between electrons, working ions and impurity ions. So we look at fluxes of particles, momentum and energy, or equivalently the corresponding diffusivity coefficients. Starting with the working particle ambipolar flux Γ^i, it is usually assumed (note superscript i denotes a working ion component) that

$$\Gamma^i = -D \quad n + nv^i$$

where D^i is the diffusion coefficient, v^i a convection velocity and n the density. By working particle we mean the primary ion species, e.g. H^+, not an impurity such as C. Theoretically, the term nv^i is expected from off-diagonal terms in the transport matrix relating transport fluxes to gradients of plasma parameters. Since both D^i and v^i can depend on fluctuation levels which in turn can depend on density gradients, the flux Γ^i cannot necessarily be partitioned into a diffusive and a convective term. However, the separation is commonly used. Γ^i is determined experimentally from spectroscopic measurements of the particle source S (using H_α light emission) by invoking continuity:

$$\frac{\partial n}{\partial t} = - \quad \cdot \Gamma^i + S$$

Behind a limiter, parallel and perpendicular flow can be balanced to derive a radial diffusion coefficient $D^i \approx 1\ m^2s^{-1}$. In the plasma interior the coefficients D^i and v^i are separately determined by following the time response of the density profile to a perturbation, e.g. an oscillating gas feed, density sawteeth or a pellet of solid fuel. The results again show $D^i \approx 1\ m^2s^{-1}$, while $v^i \approx 10\ ms^{-1}$; both of these values are larger than the neoclassical value $D^{i,nc} \approx 1x10^{-3}\ m^2s^{-1}$ and $v^{i,nc} \approx 1\ ms^{-1}$. The experimental values are described as being anomalous (i.e. anomalously large). However, there are some reported cases, near the plasma axis, where v^{nc} is in agreement with the experimental values.

Impurity particle fluxes are determined, like the working gas fluxes, from following time dependent perturbations. The results are also conventionally described by a diffusion coefficient D^z and a convection velocity v^z. Typical results show $D^z \approx D^i \approx 1\ m^2s^{-1} \approx 10\ D^{z,nc}$, with $D^{z,nc}$ the neoclassical value. The scalings of D^z and D^i with global plasma parameters are not the same. The technique used results in an intrinsic spatial weighting of v^z towards the plasma edge, and of D^z towards the plasma center. The inward convection velocity $v^z \approx v^{z,nc} \approx 10\ ms^{-1}$. Certain characteristic features of impurity behavior are predicted by neoclassical theory, e.g. impurity accumulation with co-neutral beam injection or pellet injection without sawteeth, and impurity expulsion with counter neutral beam injection or suitably chosen asymmetric working gas feed.

Momentum diffusivity is determined by following the response of the plasma rotation velocity to a momentum source. The results are generally interpreted in terms of an anomalous viscosity, although a neoclassical gyroviscous model has been proposed to explain the results. This mechanism does not explain rotation results from TFTR.

Thermal fluxes (q) and diffusivities (χ) are determined from an analysis of the radial profiles of input power, electron temperature T_e, ion temperature T_i, density n, radiation P_{rad}, charge exchange loss P_{cx}, and particle source S. The electron heat flux deduced (as a remainder) is always anomalously high, being typically 10^2 to 10^3 times the neoclassical prediction. Propagation of locally produced heat pulses gives a value a few times that derived from the profile analysis. Ion thermal fluxes are closer to the neoclassical predictions, but as more detailed information on $T_i(r)$ has become available, ion thermal diffusivities $\chi_i > 10\ \chi_i^{nc}$ have been found, with $\chi_i \approx \chi_e \approx 4\ D^i$ (although recent JET results show $\chi_e \approx 7\ D^i$.

Power Balance

$$\frac{\partial W}{\partial t} = P_{in} - P_{out}$$

$$P_{in} = P_{OH} + P_{NBI} + P_{RF} + P_{\text{inter-species}}$$

$$P_{out} = P_{conduction} + P_{convection} + P_{radiation} + P_{charge-exchange} + P_{ionization} + P_{\text{inter-species}} + P_{\text{parallel-flow}}$$

$$\frac{3}{2} n_e \frac{\partial T_e}{\partial t} = E_z j_{OH} - \frac{1}{r}\frac{\partial}{\partial r} r q_e - 3\frac{m_e}{m_p}\frac{n_e}{\tau_e}\left(T_e - T_i\right) - q_{rad} - q_{ion} + q^e_{injection} + q^e_{rf} - 2\gamma T_e \frac{\partial n_{\parallel}}{\partial t} - \frac{3}{2} T_e \frac{\partial n_e}{\partial t}$$

$$q_e = -n_e \chi_e \frac{\partial T_e}{\partial r} + \frac{3}{2} T_e \Gamma_e$$

$$\Gamma_e = \sum_j \Gamma_{Hj} + \sum_j Z_j \Gamma_{Ij}$$

$$\frac{3}{2} n_i \frac{\partial T_i}{\partial t} = -\frac{1}{r}\frac{\partial}{\partial r} r q_i + 3\frac{m_e}{m_p}\frac{n_e}{\tau_e}\left(T_e - T_i\right) - q_{cx} + q^e_{injection} + q^e_{rf} - 2T_i \frac{\partial n_\parallel}{\partial t} - \frac{3}{2} T_i \frac{\partial n_i}{\partial t}$$

$$q_i = -n_i \chi_i \frac{\partial T_i}{\partial r} + \frac{3}{2} T_i \Gamma_i$$

Perturbative tests

Follow the time history of a pulse of density or temperature. Need localized particle or heating source.

Turbulence and Fluctuation driven fluxes

Neoclassical predictions assume that the density n, electric field E, temperature T, magnetic field b and current density j are stationary. Let the respective fluctuating quantities be represented by $\tilde{n}$, $\tilde{E}$, $\tilde{T}$, $\tilde{b}$ and $\tilde{j}$ respectively. Ignoring poloidal and toroidal asymmetries, and assuming $\omega << \omega_{ci}$, the ion cyclotron frequency, then the fluctuation driven radial fluxes (denoted by superscript f) for each species (subscript j) are given by electrostatic (superscript E) and magnetic (superscript b) terms:

Particle flux

$$\Gamma_j^f = \Gamma_j^{f,E} + \Gamma_j^{f,b}$$

$$\Gamma_j^{f,E} = \left\langle \tilde{E}_\theta \tilde{n}_j \right\rangle / B_\varphi$$

$$\Gamma_j^{f,b} = -\left\langle \tilde{j}_{\parallel j} \tilde{b}_r \right\rangle / eB_\varphi$$

Energy flux

$$Q_j^f = Q_j^{f,E} + Q_j^{f,b}$$

$$Q_j^{f,E} = \frac{3}{2} k_b n_j \frac{\left\langle \tilde{E}_\theta \tilde{T}_j \right\rangle}{B_\varphi} + \frac{3}{2} k_b T_j \frac{\left\langle \tilde{E}_\theta \tilde{n}_j \right\rangle}{B_\varphi}$$

$$Q_j^{f,b} = -\left\langle \tilde{q}_{\parallel j} \tilde{b}_r \right\rangle / B_\varphi$$

Energy Confinement time

$$\tau_E \approx \frac{a^2}{D}, \quad D = \frac{\Delta^2}{\tau}.$$

Ideal: Thermal conduction and convection of ions due to binary particle collisions dominate the confinement time, and

$$\tau_E \approx \frac{a^2}{D} \approx \frac{a^2 \tau_i}{\rho_i^2 q^2 (R/a)^{3/2}}$$

Experiment: τ_E is up to 1000 times smaller than classical (+ geometry) prediction.

Explanation: Turbulence? Fluctuating electric (E) and magnetic (b) fields produce random drifts.

$$D = \frac{\Delta^2}{\tau} = \tilde{v}^2 \tau_c = \tilde{v}^2 \frac{l_{||}}{v_{||}}, \quad \tilde{v} \approx \left(\frac{\tilde{E}}{B_\varphi}\right) + v_{||}\left(\frac{\tilde{b}}{B_\varphi}\right), \quad D \approx \pi q R \left[\frac{1}{v_{||}}\left(\frac{\tilde{E}}{B_\varphi}\right)^2 + v_{||}\left(\frac{\tilde{b}}{B_\varphi}\right)^2\right]$$

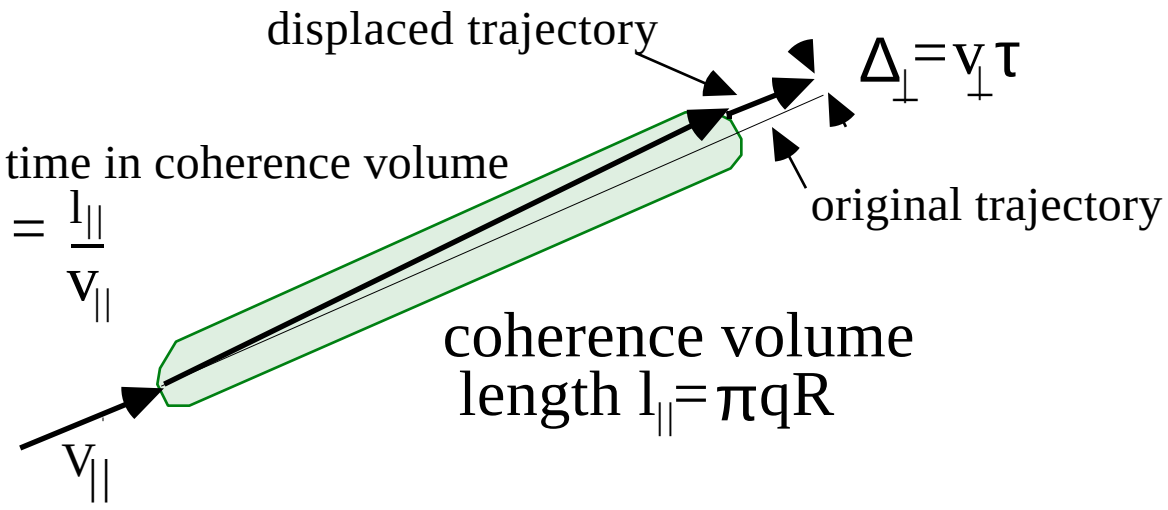

Only need very small fluctuation levels to explain the experimental confinement times.

Vu-graph on possibilities in the interior

MAGNETIC OR ELECTROSTATIC?

Magnetic?

Cannot measure directly the magnetic fluctuation driven fluxes, or even the magnetic fluctuation levels. But for high energy test particles

$$D \approx \pi q R v_{\|} \left(\frac{\tilde{b}}{B_\varphi} \right)^2$$

i.e. measure fast test particle diffusivity, and

$$\frac{D_{fast}}{D_{thermal}} \approx \frac{v_{\| fast}}{v_{\| thermal}}$$

Or Electrostatic?

$$Q_e = \frac{3}{2} \langle \tilde{p} \tilde{v} \rangle = \frac{3}{2} \frac{n}{B_\varphi} \langle \tilde{T}_e \tilde{E}_\theta \rangle + \frac{3}{2} \frac{T}{B_\varphi} \langle \tilde{n} \tilde{E}_\theta \rangle$$

i.e. measure fluctuating parameters directly

Conducted part

$$Q_{cond,e} = \frac{3}{2}\frac{n}{B_\varphi}\left\langle \tilde{T}_e \tilde{E}_\theta \right\rangle < \frac{3}{2}\frac{nT_e^2 \bar{k}}{B_\varphi}\left(\frac{\tilde{T}_e}{T_e}\frac{\tilde{\varphi}}{T_e}\right)$$

Find $\frac{\tilde{\varphi}}{T_e} \approx \frac{\tilde{n}}{n}$, so that maximum fluctuation driven heat flux is

$$Q_{cond,e}^{max} = \frac{3}{2}\frac{nT_e^2 \bar{k}}{B_\varphi}\left(\frac{\tilde{T}_e}{T_e}\frac{\tilde{n}}{n}\right)$$

Convected part

$$Q_{convect,e} = \frac{3}{2}\frac{n}{B_\varphi}\left\langle \tilde{n} \tilde{E}_\theta \right\rangle < \frac{3}{2}\frac{n^2 T_e \bar{k}}{B_\varphi}\left(\frac{\tilde{n}}{n}\frac{\tilde{\varphi}}{T_e}\right)$$

The diagnostics

"Category" indicates whether the diagnostic is to be considered day one (D1), baseline within first year(Y1), or special application (SA). "Status" represents the status of an equivalent diagnostic on TEXT-U: in normal use (N), available upon request (A), or will require modification (M) for use on USTX.

Table. Proposed USTX diagnostics grouped by the parameter measured.

Plasma Parameter	**Category**	**Status**	**Proposed Diagnostic**
Plasma Current,	D1	N	Magnetics
Position, and Shape	D1	N	CCD Camera
Control	D1	N	H_α Detectors
	D1	N	Soft X-ray Arrays
n_e	D1	N	2 mm Interferometer
	D1		Reflectometry
	Y1	M	Far-infrared Interferometry
MHD Activity	D1	N	Magnetics
	Y1	N	Soft X-ray Arrays
	SA	A	Heavy Ion Beam Probe
Hard X-rays	D1	N	Hard X-ray Detector
Limiter Heating	D1	N	Infrared Camera
	D1	N	Thermocouples
n_i	Y1	N	Spectroscopy
	SA	A	Charge-exchange (Neutral Particle)
n_Z	Y1	N	Spectroscopy
	SA	A	Charge-exchange Recombination Spectroscopy
T_e	Y1	N	Thomson Scattering
	Y1	N	Soft X-ray PHA
	Y1	N	Soft X-ray Diode Array
T_i	SA	A	Charge-exchange Recombination Spectroscopy
	Y1	N	VUV/UV Spectroscopy
Plasma potential φ	SA	A	Heavy Ion Beam Probe

Table. (continued)

Plasma Parameter	**Category**	**Status**	**Proposed Diagnostic**
Current density $J(r)$	SA	A,M	Faraday rotation
	SA	A	Charge-exchange q diagnostic
	SA		Magnetic reconstruction
	SA	A	Heavy Ion Beam Probe
Energy Content, β	D1	N	Diamagnetic Loop
	Y1	N	Thomson Scattering + magnetics
P_{rad}	Y1	N	Bolometers
	Y1	N	Spectroscopy
	SA	N	X-UV Photodiodes
Core fluctuations $\tilde{n}_e$	SA	A,M	Far-infrared Scattering
	Y1		Microwave Reflectometry
	SA	A	Beam Emission Spectroscopy
	SA	A	Heavy Ion Beam Probe
	SA	M	Phase Contrast Imaging
Core fluctuations $\tilde{\varphi}$	SA	A	Heavy Ion Beam Probe
Core fluctuations $\tilde{T}_e$	SA	D	Dual-laser Thomson Scattering
Edge fluctuations $\tilde{n}_e$	Y1	N	Electrostatic probes (also for $\tilde{T}_e$)
	Y1	A	H_α diagnostics
	SA	A	FIR Scattering
Edge fluctuations $\tilde{\varphi}$	Y1	N	Electrostatic probes
Rotation velocity	Y1	A	Spectroscopy
	Y1	A	Mach Probes
	Y1	A	Electrostatic probes
	SA	A	Charge-exchange Recombination Spectroscopy
	SA	A	Heavy Ion Beam Probe
	SA	A	FIR Scattering
Divertor & Edge	Y1	N	Electrostatic Probes
	Y1	A	Tile Probes
	Y1	N	Spectroscopy
	SA	A	Retarding Field Energy Analyzer
	D1	N	H_α monitors
	D1	N	CCD Camera
	D1	N	Fast neutral pressure gauge
	D1		Thermocouples
	SA	N	Divertor Thomson Scattering
	D1	N	Bolometers

Figures show the port allocations presently envisioned for the principal diagnostics. First figure shows a top view of USTX with the neutral-beam injector, the location of the major diagnostics, and the fast-wave current-drive antennas.

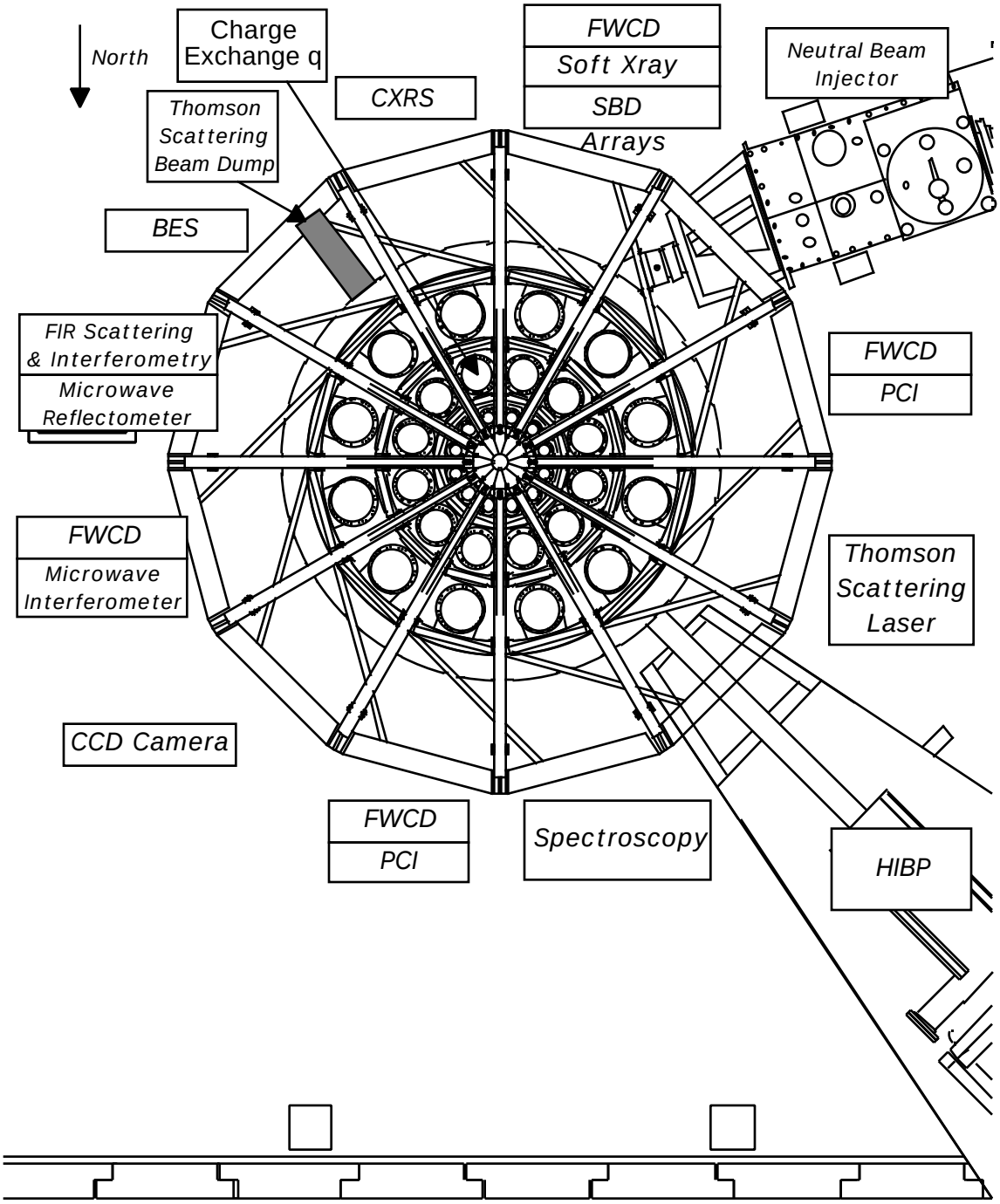

Figure. Plan view of USTX showing layout of largest diagnostics.

Second figure is a combination projection of the USTX ports in θ-φ space, showing simultaneously the top, side, and bottom ports. The north half of USTX is shown above the south half. Again, only the principal diagnostic locations are indicated.

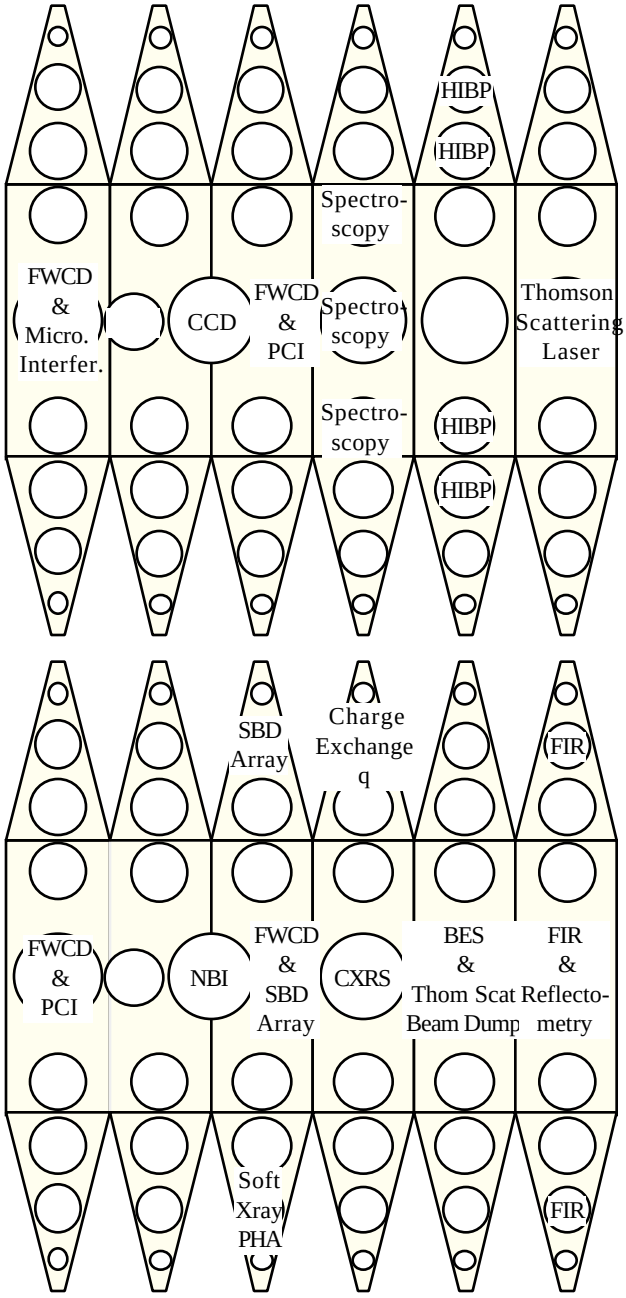

Figure. Exploded view of the 12 segments with diagnostic port assignments.